EXPERIMENTAL RESULTS IN THE EXTENDED HIGGS SECTOR*

Lino Gerlach

on behalf of the ATLAS Collaboration

II. Physikalisches Institut, Georg-August-Universität Göttingen, Germany

(Received May 13, 2020)

An Extended Higgs sector could solve many problems of the Standard Model and is, therefore, investigated by several analyses of the ATLAS experiment at the LHC. Selected searches for additional Higgs bosons and other predicted effects of an extended Higgs sector based on 139 fb^{-1} of data taken between 2015 and 2018 at a center-of-mass energy of 13 TeV are summarized.

DOI:10.5506/APhysPolB.51.1333

1. Introduction

The Standard Model of particle physics (SM) has been tested at many different experiments and, so far, every measurement made is consistent with its predictions. However, certain observations indicate that physics beyond the Standard Model (BSM) must exist. Extensions of the SM Higgs Sector could solve some of these inconsistencies — for example, by providing a candidate for dark matter or solving the hierarchy problem. Furthermore, they are a necessary premise for any supersymmetric (SUSY) extension of the SM.

A very simple SUSY theory is known as the Minimal Supersymmetric Standard Model (MSSM) [1]. It assumes two instead of one Higgs doublet leading to eight degrees of freedom. Like in the SM, after electroweak symmetry breaking, three of them are absorbed leading to five mass eigenstates that could be observed as new particles. These are denoted as $h, H, A, H^{\pm}$, where h is usually identified as the SM-like Higgs particle with a mass of 125 GeV. $H^{\pm}$ are hypothetical charged Higgs bosons and $H(A)$ would be a CP-even (odd) and electrically neutral state. With some assumptions motivated by phenomenology, the Higgs sector in the MSSM can be described at

* Presented at XXVI Cracow Epiphany Conference on LHC Physics: Standard Model and Beyond, Kraków, Poland, January 7–10, 2020.

tree level using only two parameters. These are usually chosen as m_A and $\tan\beta = \frac{\langle H_u^0 \rangle}{\langle H_d^0 \rangle}$, the ratio of the expectation values of the two Higgs doublets.

An extended Higgs sector could lead to different detectable effects at the Large Hadron Collider (LHC). For a start, it might lead to modifications of the properties of the SM-like Higgs boson with a mass of 125 GeV and its couplings. The presence of additional scalar bosons is another possibility. Furthermore, other new particles that interact with the Higgs sector could exist.

In the following, the current state of experimental results from the ATLAS detector [2] in the extended Higgs sector is summarized. Then, recent results of six different analyses are presented, two of which are based on the full Run 2 dataset.

2. Current state

So far, all measurements of the properties of the 125 GeV Higgs boson are consistent with the predictions of the SM. Furthermore, searches for additional Higgs bosons have not shown any significant deviations from the SM [3] background. In figure 1, regions of the $[m_A, \tan\beta]$ plane of the hMSSM scenario [3] that are excluded at a 95% confidence level are displayed.

However, results based on the full Run 2 dataset are able to access new regions of the phase space. A first wave of these is currently being published.

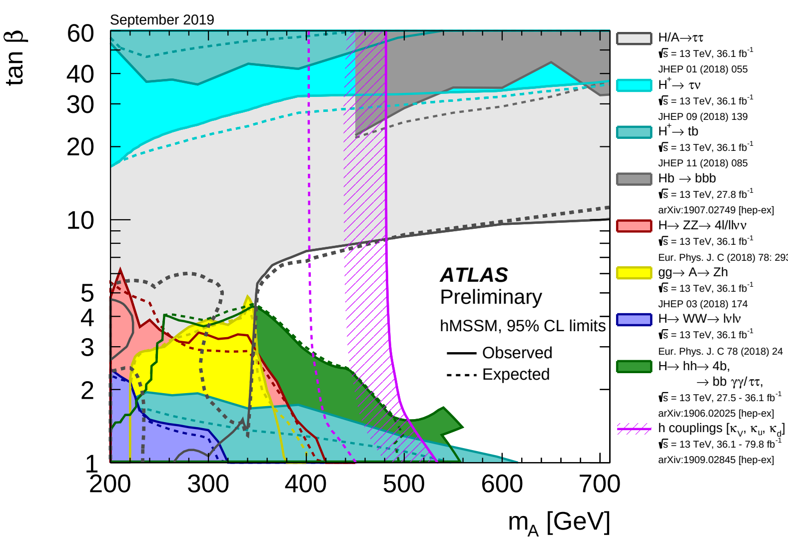

Fig. 1. Excluded regions of the $[m_A, \tan\beta]$ plane in the hMSSM scenario [4].

3. Latest results

All results shown in the following involve 13 TeV proton–proton collisions recorded at ATLAS. They cover different recent results from a variety of topics: searches for heavy Higgs, di-Higgs searches, flavour violation in the Higgs sector, and invisible or exotic decays.

3.1. Searches for heavy Higgs

3.1.1. BSM $A/H \to \tau\tau$

This analysis focuses on H/A bosons as mentioned in Section 1. High values of $\tan\beta$ will enhance the coupling of H/A to down-type fermions which is why the search for decays into pairs of τ leptons is very promising. This effect will also increase the fraction of such particles produced in association with b-quarks. In figure 2, all production modes that are considered in this analysis are shown. The considered data consist of 36 fb^{-1} of integrated

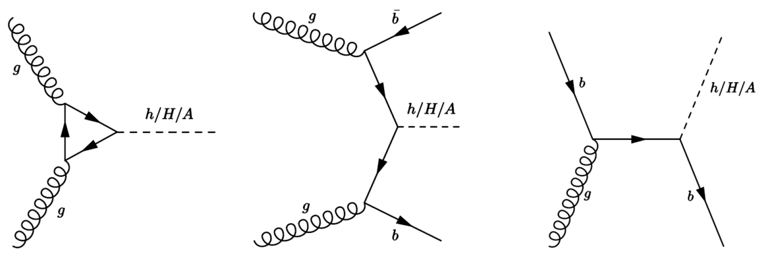

Fig. 2. Strong Higgs production via gluon–gluon fusion and b-associated production with and without, and incoming b-quark (from left to right) [5].

luminosity with a center-of-mass energy of 13 TeV. The analysis is split into a fully hadronic (hadhad) and a semi-leptonic (lephad) channel. Events were selected by a single lepton and a single tau trigger, respectively. In order to exploit the different production modes, the Signal Region (SR) is split into a b-veto and a b-tag category. The total transverse mass as defined in

$$m_{\mathrm{T}}^{\mathrm{tot}} = \sqrt{m_{\mathrm{T}}^2(E_{\mathrm{T}}^{\mathrm{miss}}, \tau_1) + m_{\mathrm{T}}^2(E_{\mathrm{T}}^{\mathrm{miss}}, \tau_2) + m_{\mathrm{T}}^2(\tau_1, \tau_2)} \tag{1}$$

is used as a final discriminant. Its distribution in the b-veto category can be seen in figure 3 for the lephad and the hadhad channel, separately. The three main backgrounds are estimated as follows. For misidentified tau leptons from multijet events, a data-driven technique known as the Fake Factor method is deployed. For fakes from all other processes, a semi-data-driven fake rate approach was chosen. All backgrounds containing real τ leptons are taken directly from Monte Carlo simulations.

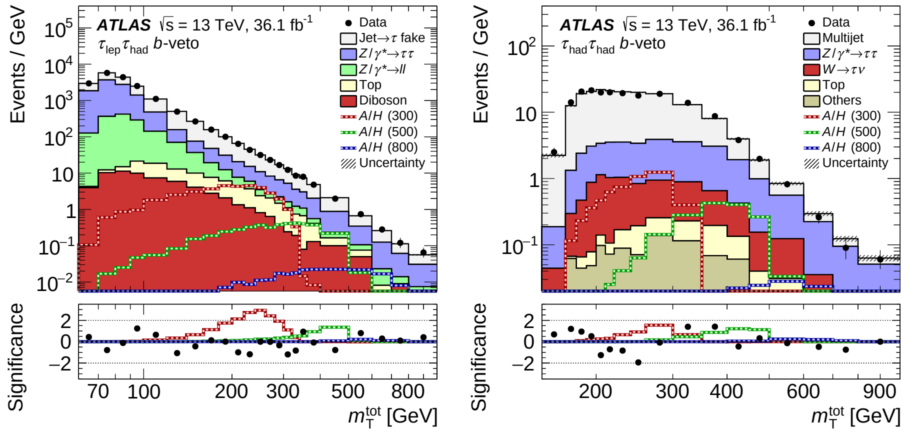

Fig. 3. The $m_{\mathrm{T}}^{\mathrm{tot}}$ distribution in the b-veto category [6].

The 95% C.L. upper limits on the production cross section times branching fraction can be seen in figure 4 alongside the corresponding limits in the $[m_A, \tan\beta]$ plane in the M_h^{125} scenario [3].

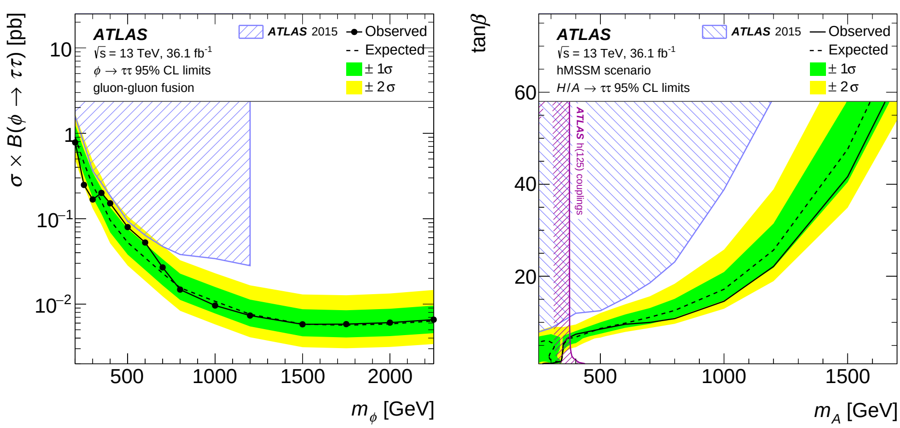

Fig. 4. The observed and expected 95% C.L. upper limits on the production cross section times branching fraction (left) and on $\tan\beta$ as a function of m_A in the M_h^{125} scenario [6].

3.1.2. BSM $bH(H \to bb)$

This analysis focuses on the production of a heavy neutral scalar in association with a b-quark where the scalar decays into a pair of b-quarks. Some of the production processes considered are displayed in figure 5. Similarly

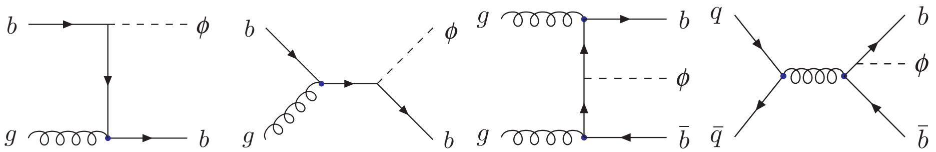

Fig. 5. Feynman diagrams for some of the leading-order processes for the production of a heavy neutral Higgs boson in association with one or two b-quarks in the 5-flavour scheme [7].

to the analysis in Section 3.1.1, this search is sensitive to high values of $\tan\beta$. All in all, 27.8 fb^{-1} of data are considered. For the event selection, a single jet trigger is required to have fired at Level 1. For the High Level Trigger, a logical OR between a single ($E_{\mathrm{T}} > 225$ GeV) and a double b-tag trigger is implemented. The SR is split into six subregions based on the number of jets (4, 5, 6) and the number of b-tagged jets after reconstruction ($n_b \geq 3$: bbb region, $n_b = 2$: bb anti-region). Due to the final-state radiation (FSR) of the b-jets, the reconstructed mass of the two b-jet system, m_{bb}, is heavily smeared. The goal is to isolate events with a low amount of FSR. To achieve this, correlations between three different kinematic variables are used: The transverse momentum of the (sub-)leading b-jet $p_{\mathrm{T1(2)}}$, and m_{bb} are exploited. In figure 6, p_{T1} is plotted *versus* m_{bb} for multijet background and a hypothetical signal. To exploit the correlations, a principle component analysis (PCA) is conducted. Here, the three input variables are linearly combined to construct the new variable m'_{bb} that possesses the best separation power. This new variable is then used for a simultaneous fit in all 6 subcategories with a freely floating background normalisation. The multijet contribution in the bb-anti regions is used as a template in the

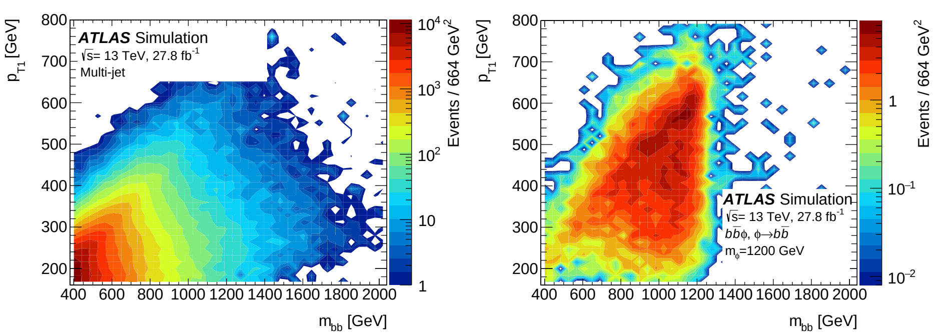

Fig. 6. Two-dimensional distributions of p_{T1} *versus* m_{bb} for events with the bbb classification following preselection, summed over all three N_{jet} regions. Plots are shown for multijet MC (left) and for data (right) [7].

bbb SR. This procedure is repeated for every tested mass point, ending up in 15 different definitions for m'_{bb} and independent fits. The results are presented as 95% C.L. upper limits on cross section times branching ratio and in the $[m_A, \tan\beta]$ plane in the MSSM for different scenarios in figure 7.

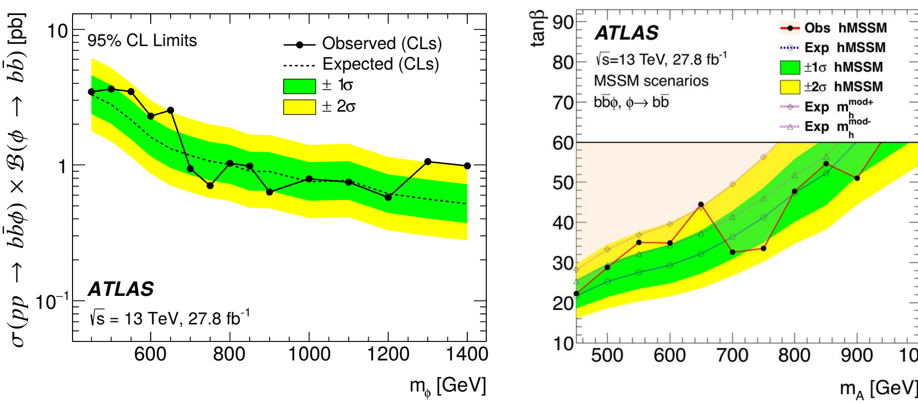

Fig. 7. Observed and expected upper limits on production cross section times branching fraction at 95% C.L. as a function of the Higgs boson mass (left) in the $[m_A, \tan\beta]$ plane in the MSSM for different scenarios [7].

3.2. Di-Higgs searches

Searches for processes with two Higgs bosons (di-Higgs) are of special interest for an extended Higgs sector. Not only would a hypothetical heavy enough resonance be able to decay into two SM-like bosons, the non-resonant production itself may also be sensitive to BSM effects. The possible final states of a di-Higgs system with a high expected branching ratio ($4b$ and $bbWW$) have challenging backgrounds, while the decay channels with a clear signature have very low expected branching fractions (*e.g.* 4γ). Therefore, there is no single channel that dominates the sensitivity, thus searches are currently investigating a plethora of different possible final states.

3.2.1. VBF $hh \to 4b$

One di-Higgs search that has recently published a new result recently is investigating pairs of Higgs bosons produced via vector boson fusion (VBF) that then decay exclusively into b-quarks. The decay of two Higgs bosons into four b-jets in the final state has the highest expected branching ratio but a very challenging background. The VBF production processes at tree level are displayed in figure 8. Interference between the resonant and non-resonant production diagrams may lead to a lower production cross section than in the SM-like exclusively non-resonant case. The analysis considered 126 fb^{-1}

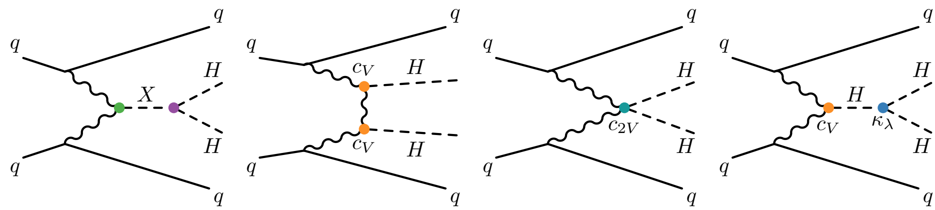

Fig. 8. Tree-level Feynman diagrams contributing to Higgs boson pair production via VBF. The resonant (left) and non-resonant production modes scaling with c_{2V} and κ_λ are displayed [8].

of data taken between 2016 and 2018. Events were selected by a combination of 4 b-jet triggers. After reconstruction, there must be at least four central b-jets as well as two forward jets satisfying $|\eta| > 2.0$. The signal is then isolated by cuts on the jet kinematics that split the event selection into signal, validation and side band regions. For this, a system of inequations is implemented involving the invariant mass of the (sub-)leading two-b-jet system, $m_{2b}^{(\mathrm{sub-})\mathrm{lead}}$, the invariant mass of the four-b-jet system, m_{4b}, as well as the distance between the two b-jets in each subsystem, $\Delta R_{2b}^{(\mathrm{sub-})\mathrm{lead}}$. In figure 9, the different regions are graphically displayed as ellipses in the $[m_{2b}^{\mathrm{lead}}, m_{2b}^{\mathrm{sublead}}]$ plane alongside the distributions for a SM-like signal and the multijet background. In order to extract limits on the production cross section times branching ratio, a fit in m_{4b} is conducted where the SM-like (background only) hypothesis is fitted to the observed data which can be seen on the left in figure 10. Limits are set for a broad and a narrow resonance, separately.

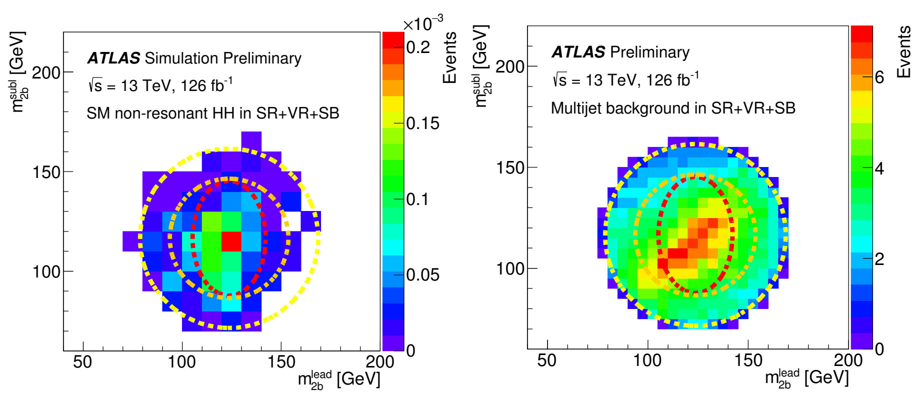

Fig. 9. (Colour on-line) Two-dimensional mass regions used in the analysis. The SR is inside the inner (red) dashed curve, the validation region is outside the signal region and within the intermediate (orange) circle, the side band is outside the validation region and within the outer (yellow) circle [8].

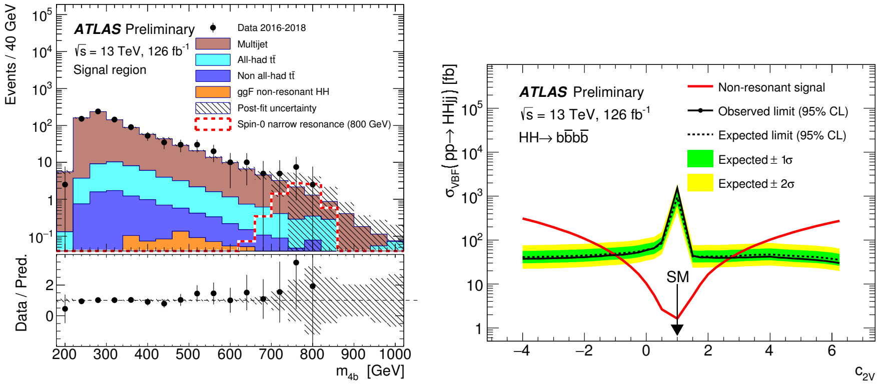

Fig. 10. Mass distribution of the HH candidates in the SR after the profile-likelihood fit to data with the background-only hypothesis (left) and observed and expected 95% C.L. upper limits on the production cross section for non-resonant HH production via VBF as a function of the $HHVV$ coupling c_{2V} [8] (right).

3.3. Flavour violation

3.3.1. BSM $H(125) \to e\mu/ee$

This analysis searches for the decay of a 125 GeV Higgs boson into two electrons as well as the lepton flavour conservation violating decay into an electron and a muon. The Feynman diagrams for these decays can be seen in figure 11 for the two leading production mechanisms.

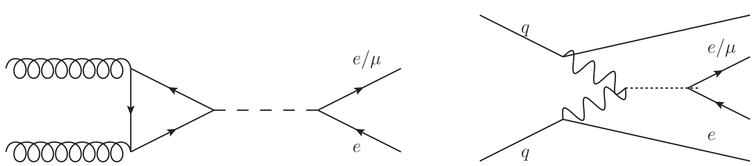

Fig. 11. Feynman diagrams for $H \to e\mu/ee$ in the VBF (left) or ggF production channel (right).

The full 139 fb^{-1} of Run 2 data are considered. Events are selected with a single electron (muon) trigger. Additionally, some kinematic cuts are applied along with a b-veto. The low and high p_{T} signal regions are split by a p_{T} requirement on the leading lepton. If events in the high p_{T} category contain two jets in opposite hemispheres, they are classified as VBF. All other high p_{T} events define the ggF category which is also split into a central and a non-central subcategory based on $|\eta|$ of both leptons. In total, there are four SRs for each decay channel. The invariant mass of the two-lepton system, m_{ll}, is used as the final discriminant. Its distribution in the $ee(\mu)$ channel can be seen in figure 12 on the left (right) for data, background and a hypothetical signal with an assumed branching fraction of 2(0.05)%. The Higgs mass window is chosen to be $110 < m_{ll} < 160$ GeV. The side bands are used

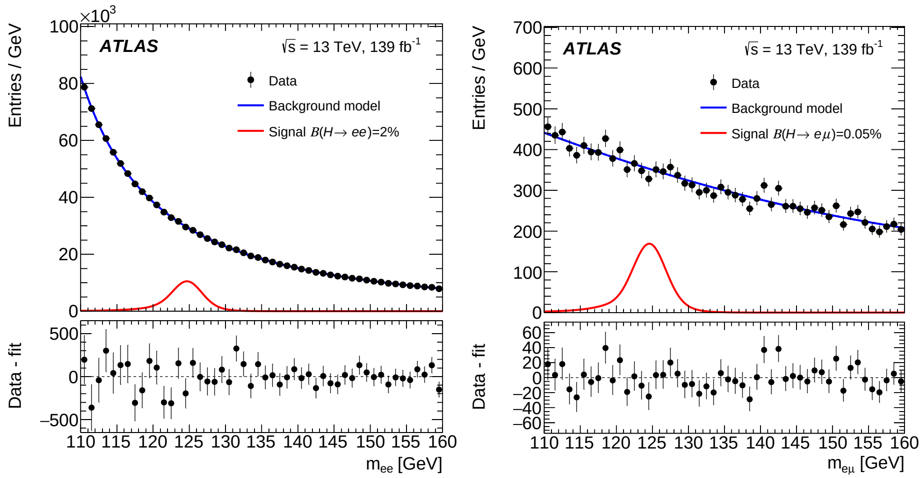

Fig. 12. (Colour on-line) Likelihood fits to the m_{ll} distribution in data (points) using the background model (black/blue line) for all categories. A goodness of fit is tested by evaluating a χ^2 value for each category based on statistical errors only. The signal parametrisation with a branching fraction set to $B(H \to ee) = 2\%$ is also shown (grey/red line) [9].

as a CR. The backgrounds are described by analytic functions and fitted to the data. Results are presented as scans of the C.L. in dependence of the respective branching fraction as can be seen in figure 13. The 95% C.L.

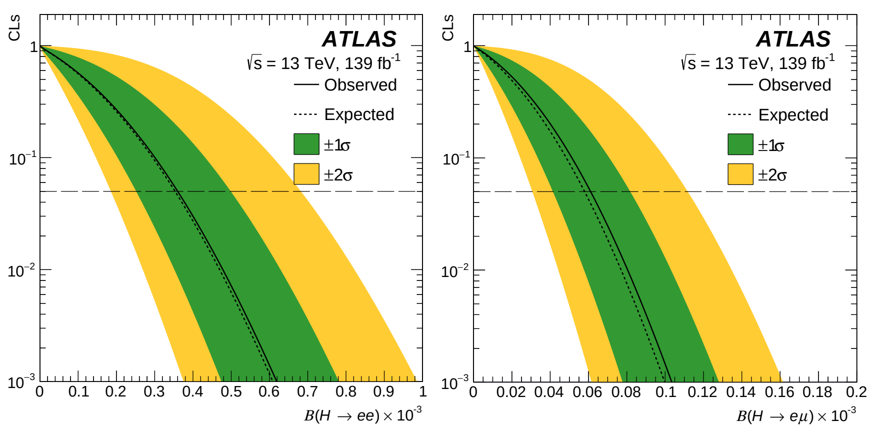

Fig. 13. CL_s scans in the ee (left) and $e\mu$ (right) channels [9].

upper limit on the branching fractions are 3.6×10^{-4} and 6.1×10^{-5} for the ee and the $e\mu$ channel, respectively. This marks a strong improvement compared to the previous best results of 1.9×10^{-3} and 3.5×10^{-4} based on 36.1 fb^{-1} of data.

3.4. Invisible/exotic decays

3.4.1. $H(125) \rightarrow$ invisible combination

As mentioned in Section 1, couplings of new, unknown or invisible particles to the 125 GeV Higgs boson are also considered part of an extended Higgs sector. In a recently published result, three different searches for invisible Higgs decays were combined. In the first one, the Higgs boson is assumed to be produced in a VBF process. The other two searches focus on Higgs bosons produced in association with a vector boson where the vector boson decays leptonically $Z(\mathrm{lep})H$ or hadronically $V(\mathrm{had})H$, respectively. $E_{\mathrm{T}}^{\mathrm{miss}}$ triggers are required to have fired for the VBF and the $V(\mathrm{had})H$ channels. Any single lepton trigger marks an event for the $Z(\mathrm{lep})H$ channel. All three analyses impose cuts on the missing transverse energy: VBF: $E_{\mathrm{T}}^{\mathrm{miss}} > 180$ GeV, $Z(\mathrm{lep})H$: $E_{\mathrm{T}}^{\mathrm{miss}} > 90$ GeV, and $V(\mathrm{had})H$: $E_{\mathrm{T}}^{\mathrm{miss}} > 150$ GeV. $Z(\nu\nu)$+jets and $W(l\nu)$+jets are the dominant backgrounds in the VBF and the $V(\mathrm{had})H$ channel, whereas $Z(\nu\nu)Z(ll)$ and $W(l\nu)Z(ll)$ are the dominant ones in the $Z(\mathrm{lep})H$ channel. Results are presented as the negative logarithmic likelihood (LLH) ratio *versus* the branching fraction, $\mathrm{B}(H \rightarrow \mathrm{inv})$, in figure 14. The best fit values lies at $\mathrm{BR}(H \rightarrow \mathrm{inv}) = 0.13 \pm 0.08$ with a 95% C.L. observed (exp.) upper limit of $\mathrm{BR}(H \rightarrow \mathrm{inv}) < 0.26(0.17^{+0.07}_{-0.05})$.

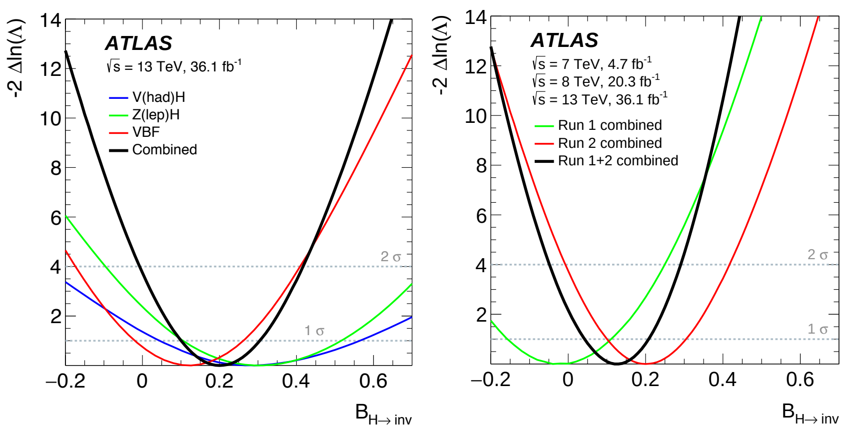

Fig. 14. The observed negative LLH ratios $-2\Delta\ln(\Lambda)$ as a function of $\mathrm{B}(H \rightarrow \mathrm{inv})$ of the $V(\mathrm{had})H$, $Z(\mathrm{lep})H$, and VBF topologies using Run 2 data only and their statistical combination (left). The $-2\Delta\ln(\Lambda)$ functions for the Run 2 combination together with the Run 1 combination and the total Run 1+2 combination (right) [10].

4. Conclusion and outlook

Thus far, ATLAS results are compatible with the SM-like Higgs scenario. However, there is still room for BSM physics in the Higgs sector. For one, additional heavy Higgs bosons could hide at higher masses that have simply not yet been accessed. Other effects of an extended Higgs sector are expected to be so rare that analyses will only become sensitive with more data.

In any case, exciting times lie ahead and ATLAS is looking forward to Run 3 and the High-Luminosity LHC.

REFERENCES

[1] S.P. Martin, *Adv. Ser. Direct. High Energy Phys.* **18**, 1 (1998), arXiv:hep-ph/9709356.

[2] ATLAS Collaboration, *JINST* **3**, S08003 (2008).

[3] M. Carena *et al.*, *Eur. Phys. J. C* **73**, 2552 (2013), arXiv:1302.7033 [hep-ph].

[4] ATLAS Collaboration, «hMSSM summary plots from direct and indirect searches», Technical Report ATL-PHYS-PUB-2020-006, CERN, Geneva, March 2020, http://cds.cern.ch/record/2713580

[5] ATLAS Collaboration, «Search for minimal supersymmetric Standard Model Higgs bosons H/A in the $\tau\tau$ final state in up to 13.3 fb^{-1} of pp collisions at $\sqrt{s} = 13$ TeV with the ATLAS Detector», ATLAS-CONF-2016-085, 2016.

[6] ATLAS Collaboration, *J. High Energy Phys.* **1801**, 055 (2018), arXiv:1709.07242 [hep-ex].

[7] ATLAS Collaboration, arXiv:1907.02749 [hep-ex].

[8] ATLAS Collaboration, «Search for the $HH \to b\bar{b}b\bar{b}$ process via vector boson fusion production using proton–proton collisions at $\sqrt{s} = 13$ TeV with the ATLAS detector», Technical Report ATLAS-CONF-2019-030, CERN, Geneva, July 2019, http://cds.cern.ch/record/2682801

[9] ATLAS Collaboration, *Phys. Lett. B* **801**, 135148 (2020), arXiv:1909.10235 [hep-ex].

[10] ATLAS Collaboration, *Phys. Rev. Lett.* **122**, 231801 (2019), arXiv:1904.05105 [hep-ex].